

Effect of Friction Stir Welding Parameters on the Peak Temperature and the Mechanical Properties of Aluminum Alloy 5083-O

Mostafa M. El-Sayed, Ahmed Y. Shash, Tamer S. Mahmoud
and Mahmoud Abd Rabbou

Abstract In the present investigation, a 3D transient heat transfer model is developed to simulate the thermal distribution of aluminum alloy 5083-O friction stir welded by using Abaqus software. A 6 mm AA5083-O plates were friction stir welded at different conditions; two tools with tapered smooth and cylindrical threaded pin profiles, and 50, 100, 160 mm/min welding speeds at a constant rotational speed of 400 rpm. The temperature was measured using an infrared thermal image camera during the welding process at each operation condition. The measured temperature by IR camera was compared with temperatures obtained using the Abaqus. The welded joints were checked by visual inspection, macrostructure and microstructure evolution, in addition to tensile strength and hardness profiling. The welding speed and tool pin profile variations have a small effect on the peak temperature of the welded joints. The defect free welded joints were obtained at 50, 100, 160 mm/min welding speeds using a threaded tool pin profile. The tensile strength values obtained by using a threaded tool pin profile at all welding speeds are better than those obtained by using a tapered tool pin profile where the best one is at 50 mm/min welding speed. In terms of hardness results, the threaded tool pin profile gives better results at all welding speeds than the tapered tool pin profile.

Keywords Friction stir welding • Tool pin profile • Mechanical properties • Finite element modeling

M.M. El-Sayed · A.Y. Shash (✉) · T.S. Mahmoud · M.A. Rabbou
Mechanical Design and Production Engineering Dept, Cairo University,
Giza 12311, Egypt
e-mail: ahmed.shash@cu.edu.eg

M.M. El-Sayed
e-mail: mostafamohammed30@yahoo.com

M.A. Rabbou
e-mail: mahmoud.abdrabbou@gmail.com

1 Introduction

Friction Stir Welding (FSW) was invented by Wayne Thomas at TWI (The Welding Institute), in the UK in 1991. FSW is a solid state joining process, in which the objects are welded together without reaching the melting point of the base metal [1].

In FSW, a non-consumable shouldered tool with a profiled pin is rotated and immersed into the abutting faces of work-pieces, thereby generating frictional heating at tool-work piece interface, leading to softening of the work-piece material. After that, the tool is moved along the joint line producing a continuous welded joint [2].

FSW is considered to be environmentally friendly because there is no cover gas. Since no melting occurs during FSW, it can be used for joining the 2xxx and 7xxx aluminum alloys which are difficult to weld using traditional methods due to the poor solidification of the microstructure and porosity in the fusion zone. Also, it can be used for welding any kinds of materials, material composites, and dissimilar materials, with ease [3].

These days, FSW is applied in many industries such as: aerospace, shipbuilding and automotive industries [4].

There are many parameters affecting the mechanical properties and microstructure of friction stir welded joints. These parameters are: tool design, rotational speed, welding speed, axial force, plunge depth and tool tilt angle. Rotation speed affects the frictional heat, welding speed control which affects the heat generated, tool tilt angles which affects the efficiency of the weld, plunge depth which produces sound welds, axial force which generates further heating and tool design which affects the flow and the power required for the process [5].

The microstructure of aluminum friction stir welded joints is classified into four zones. This classification is based on the effect of the heat and plastic deformation on the material. These zones are: the first one is an unaffected zone in which neither heating nor plastic deformation affect the microstructure of the material. The second one is the heat affected zone (HAZ) which is adjacent to the unaffected zone, where the heat generated has no effect on the microstructure of the material. The third one is the thermo-mechanically affected zone (TMAZ) which is adjacent to the HAZ, where both heat and plastic deformation affect the microstructure but, there is no recrystallization occurred because the deformation strain is not enough. The fourth one is the dynamically recrystallized zone (DXZ) which is lying in the weld center line beside the TMAZ and subject to both higher deformation strain and higher temperature which cause recrystallization of the material resulting in finer grains sizes [6].

Many investigators [7–11] have studied and reported on the effect of FSW parameters on the mechanical properties and microstructure of friction stir welded aluminum joints.

FSW has three main phases: the plunge phase, dwell phase and welding phase [7]. The generated heat from the FSW process is frictional heat and plastic dissipation heat generation. The first one is due to the contact between the tool and work-piece, while the second one is due to plastic energy dissipation [12].

Since FSW has both thermal and mechanical loads, simulation of that process is quite complicated to obtain the thermal history and stresses produced from it. Some investigators have built a heat transfer model to predict the temperature distribution during the FSW process, while others have built a thermo-mechanical model to simulate the plunge phase during the process. However, a few investigators have built a heat and material flow models to simulate the flow of material during the process [13].

2 Experimental Investigations

2.1 Numerical Simulation

A 3D transient heat transfer finite element model was developed to simulate the thermal distribution during friction stir welding of AA5083-O using the Abaqus software. The part dimensions are 100 × 50 × 6 mm for one piece where half of welding was simulated to reduce running time. The heat losses due to convection and radiation are neglected. Temperature dependent properties of the model are shown in Table 1.

Boundary conditions (BCs): the model is completely fixed in all directions except along the welding line, where it is partially fixed.

Load: a heat flux load is subjected to the surface of the part with a certain value. This value is obtained from the following formula:

Heat flux(Q) = \frac{heat\ input(q)}{Area(A)} (W/m^2)

Table 1 The temperature dependent properties of AA5083

Temperature	Conductivity (W/m °C)	Specific heat (J/kg °C)	Density (kg/m ³)
−20	112.5	924.1	2673.9
80	122.7	984.2	2642.7
180	131.6	1039.6	2629.4
280	142.3	1081.2	2611.5
380	152.5	1136.6	2589.3
480	159.5	1178.2	2567
580	177.2	1261.4	2549.2

Heat input (q) is calculated from the *Frigard* equation

$$q = \int_0^R 2\omega\pi\mu Pr^2 dr \text{ (W)},$$

$$\omega = \frac{2\pi n}{60}$$

$$q = \int_0^R \frac{2}{30} \pi^2 \mu P n r^2 dr = \frac{1}{45} \pi^2 \mu P n (R^3 - r^3)$$

where

ω : Angular velocity (rad/sec)

n : Rotational speed(rpm) $P = \frac{F}{A}$

The following assumptions are considered:

Friction coefficient (μ) = 0.4

Axial force (F) = 2000 N

$A = \pi(R - r)^2 \text{ mm}^2$

Shoulder radius (R) = 12.5 mm

Pin radius (r) = 4 mm

Since the friction coefficient, axial force, shoulder radius and pin radius are constants, changing the rotational speed values results in changed heat flux values leading to a change in the temperature distribution. Then, $Q = 2.5 \times 10^6 \text{ W/m}^2$ (at **400 rpm**).

Figure 1 shows both boundary conditions and load subjected to the part.

Meshing: The element type is heat transfer DCC3D8 with 8-node convection/diffusion brick. Figure 2 shows the meshing of the part.

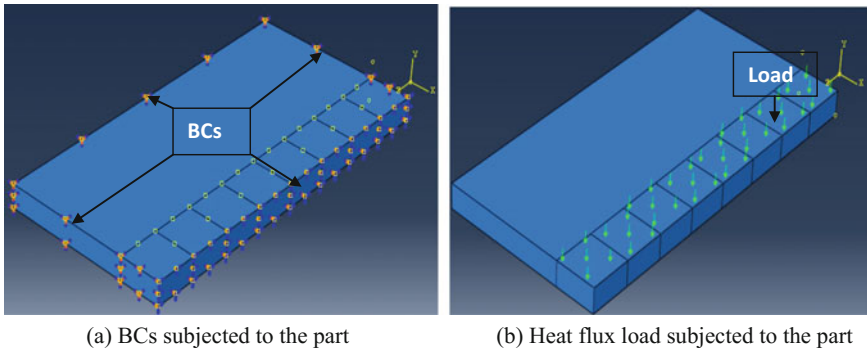
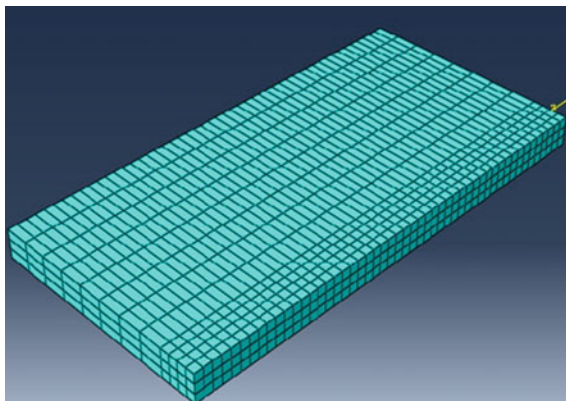


Fig. 1 BCs and load on the part

Fig. 2 Meshing of the part

2.2 Welding Process and Operation Conditions

The tool material is **K720** with **57 HRC**. Two tools with two different pin profiles, cylindrical threaded and tapered smooth pin profiles, were used. Figure 3 shows the schematic drawing of each tool. The work piece material is **AA5083-O** with dimensions of $100 \times 50 \times 6$ mm which is half of the welded joint. Tables 2 and 3 show the material chemical composition and mechanical properties respectively.

A universal milling machine was used to perform the friction stir welding process. The work piece was fixed on the machine by a mechanical vice as shown in Fig. 4. Table 4 shows the FSW parameters. **Fluke infra-red** thermal image camera shown in Fig. 5 was used to measure the temperature at each operation condition.

2.3 Material Characterization

A rectangular specimen was cut out from each friction stir welded joint perpendicular to the welding line. The samples were grinded using emery papers down to 2500 grade followed by polishing using $0.3 \mu\text{m}$ alumina suspension solution. The surfaces of the specimens were etched using Poulton's reagent [2 ml HF, 3 ml HCl, 20 ml HNO_3 , 175 ml H_2O]. The microstructure examination was carried out using an OLYMPUS optical metallurgical microscope, equipped with a high resolution digital camera for the investigation of the microstructure.

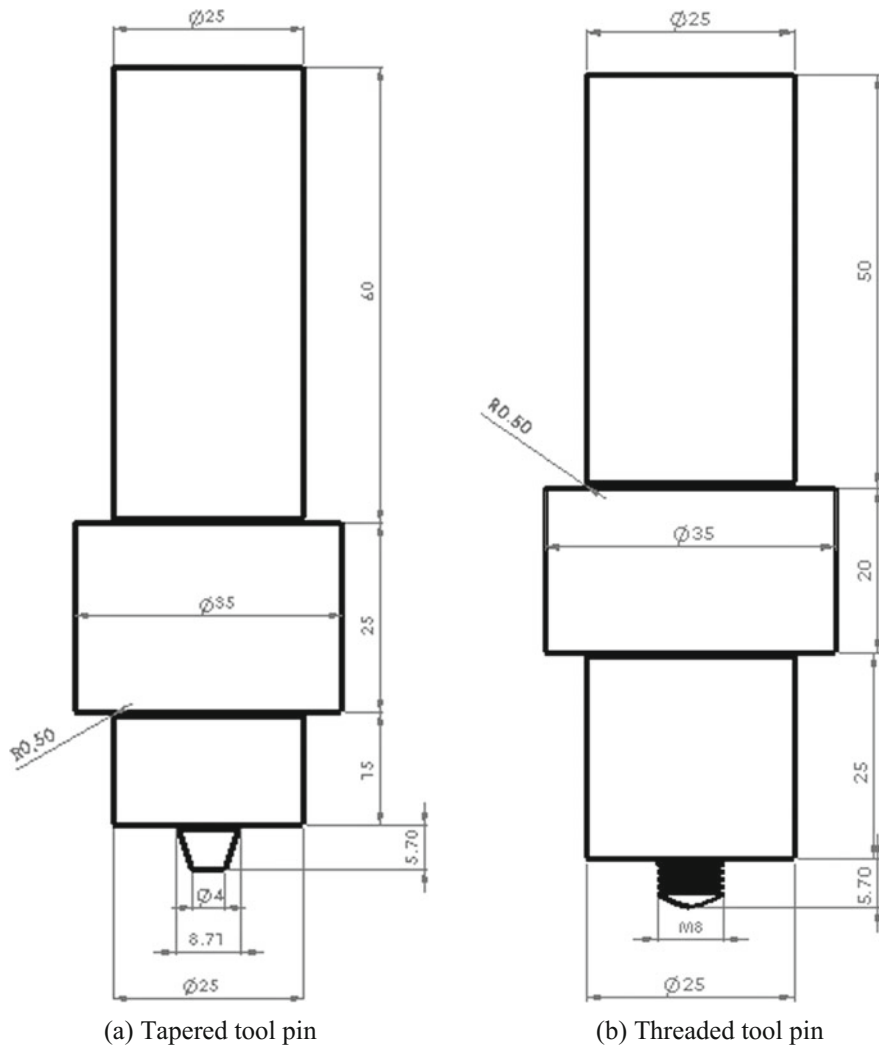


Fig. 3 Tools geometry

Table 2 The chemical composition of AA5083-O

Si	Fe	Cu	Mn	Mg	Zn	Ni	Pb	Sn	Al
0.1737	0.2867	<0.0010	0.4623	4.298	0.0075	<0.005	<0.002	<0.002	Balance

Table 3 The mechanical properties of AA5083-O

Ultimate tensile strength (σ_u)	Yield strength (σ_y)	Elongation (%)	Vickers Hardness (HV)
272	176	14	75

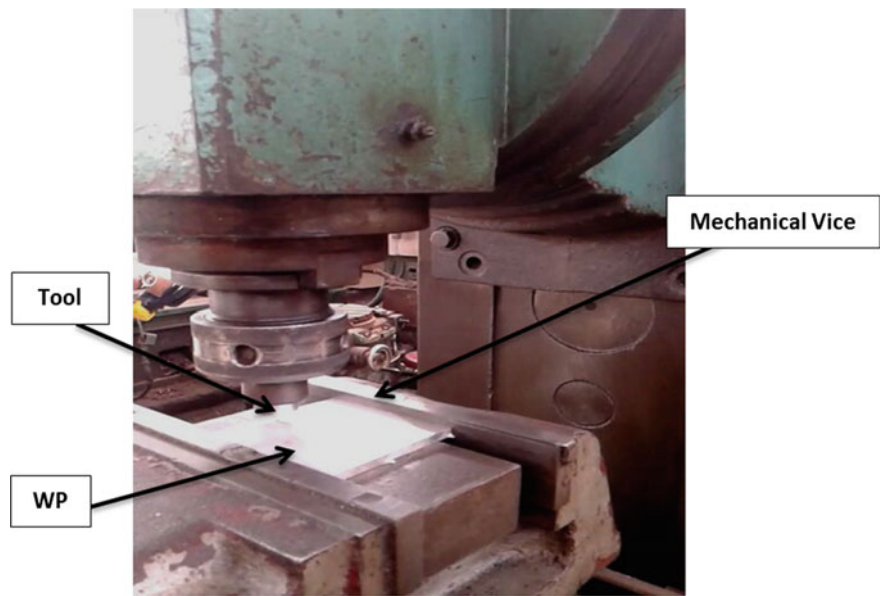


Fig. 4 Machine set-up

Table 4 FSW parameters

Process parameters	Tool pin profile	Welding speed (mm/min)	Rotational speed (rpm)	Plunge depth (mm)	Tool tilt angle (°)
Value	Cylindrical threaded and tapered smooth	50, 100 and 160	400	0.2	0

Fig. 5 Fluke IR thermal image camera



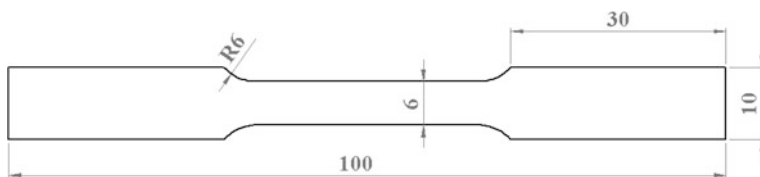


Fig. 6 Schematic drawing of tension test specimen (Thickness = 6 mm)

2.4 Mechanical Properties

The mechanical properties, mainly tensile strength and hardness, were measured for each sample.

2.4.1 Tensile Strength

Three tension test samples were taken from each welded joint and cut according to ASTM standard dimensions as shown in Fig. 6, tested on a universal testing machine and the average values were calculated for each case.

2.4.2 Microhardness Test

A rectangular specimen was cut out from each friction stir welded joint perpendicular to the welding line. The microhardness tests were conducted on a Zwick/Roell hardness testing machine.

3 Results and Discussions

3.1 Numerical Simulation and Temperature Distribution

After running the job of the model, the simulation is obtained and a path is taken along the line perpendicular to welding line to graph the temperature distribution. Figure 7a shows the temperature profile during simulation and Fig. 7b shows the temperature distribution curve obtained from simulation. It is observed that the peak temperature obtained from simulation in welding area is 448.8 °C and the temperature at 50 mm far from weld centre line is about 69.5 °C.

Figure 8 shows the variation of peak temperature at different welding speeds. It is observed from the graph that the highest peak temperature is at **50 mm/min** welding speed and the lowest one is at **150 mm/min** for the same tool pin profile. It is noticed that the tool pin profile does not strongly affect the peak temperature of the joints during welding process.

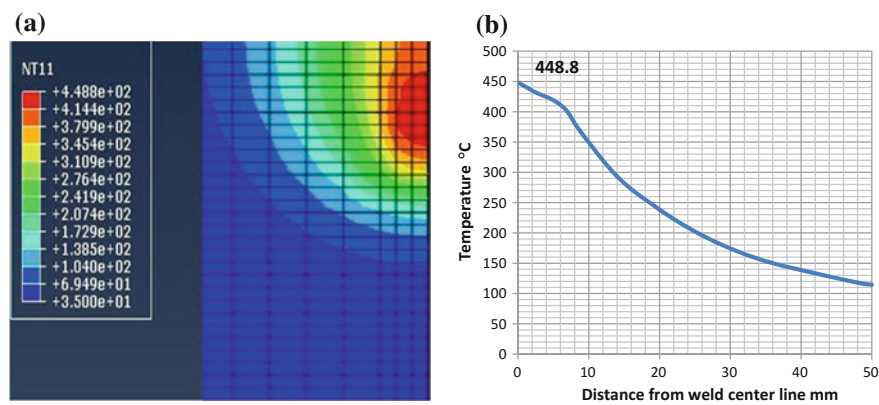


Fig. 7 a Temperature profile. b Simulated temperature distribution

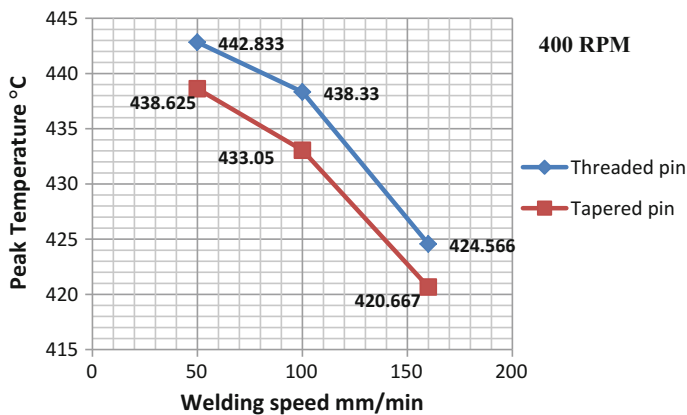


Fig. 8 Variation of peak temperature due to variation of welding speed and tool pin profile at 400 rpm

Figure 9 shows the comparison between the simulated temperature distribution obtained by the Abaqus software and the measured temperature distribution obtained by IR camera at **400 rpm** rotational speed and **50 mm/min** welding speed.

3.2 Surface Morphology

The upper surface macrographs of the welded joints at different welding conditions are shown in Fig. 10. It is observed from figure that the welded joints by threaded and tapered tool pin profile have an accepted surface appearance at all welding speeds where there are no grooves or surface-open tunnel defects.

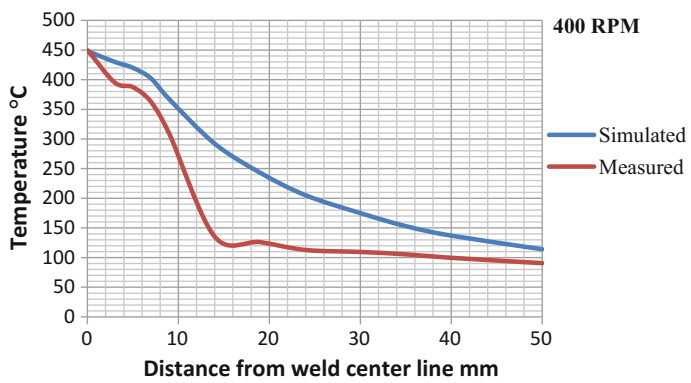


Fig. 9 Simulated and experimental temperature distribution

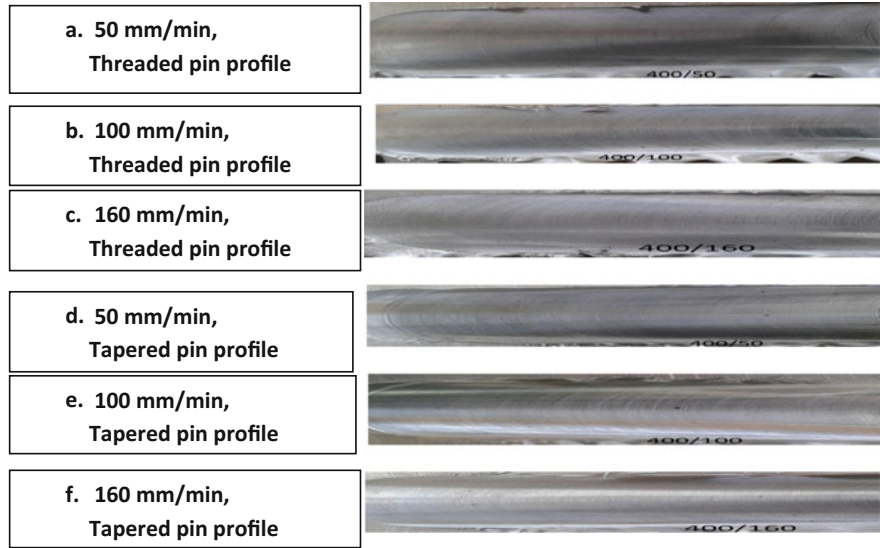


Fig. 10 Surface morphologies at different operating conditions

3.3 Macrostructure and Microstructure Evolutions

Figure 11 shows the macrostructure and microstructure observation for each sample. As observed from this figure, the defect free welds are obtained when welding process is performed using cylindrical threaded tool pin profile at all welding speeds values. While tunnel defects appeared when using smooth tapered pin

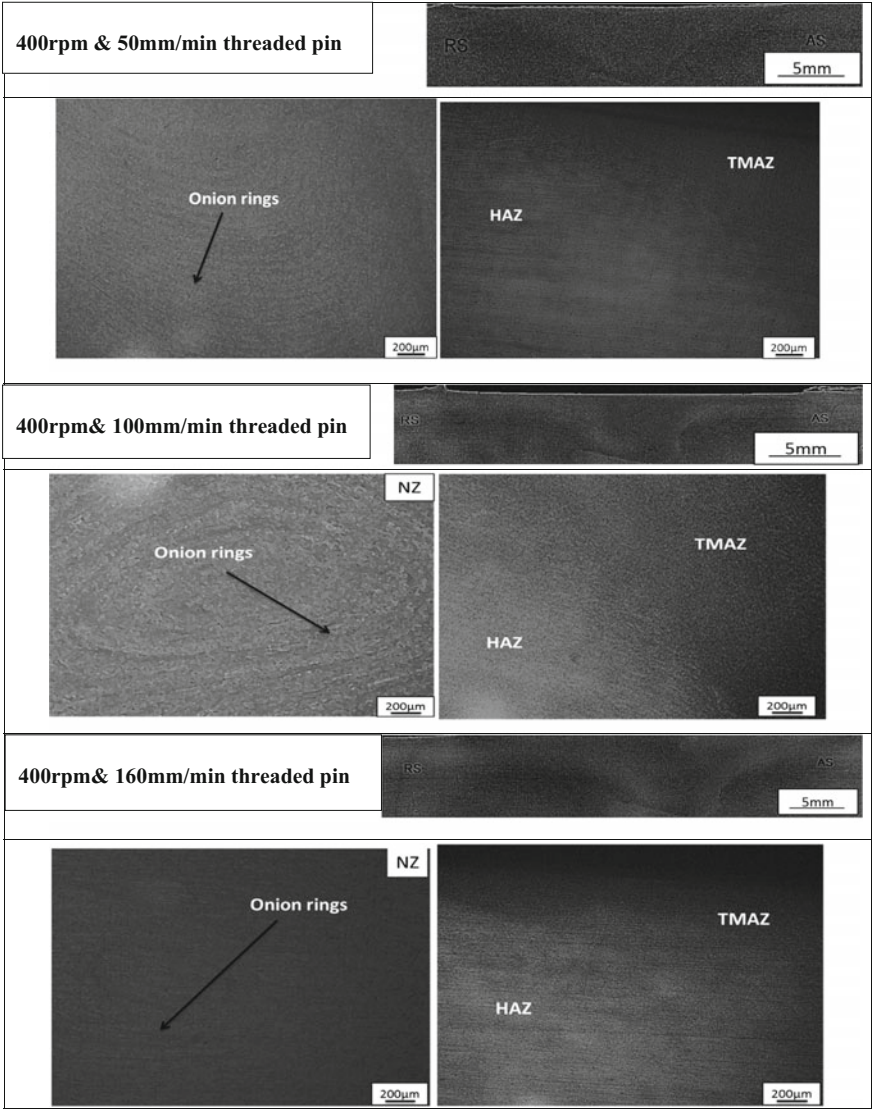


Fig. 11 Macrostructure and microstructure evolutions at different operation conditions

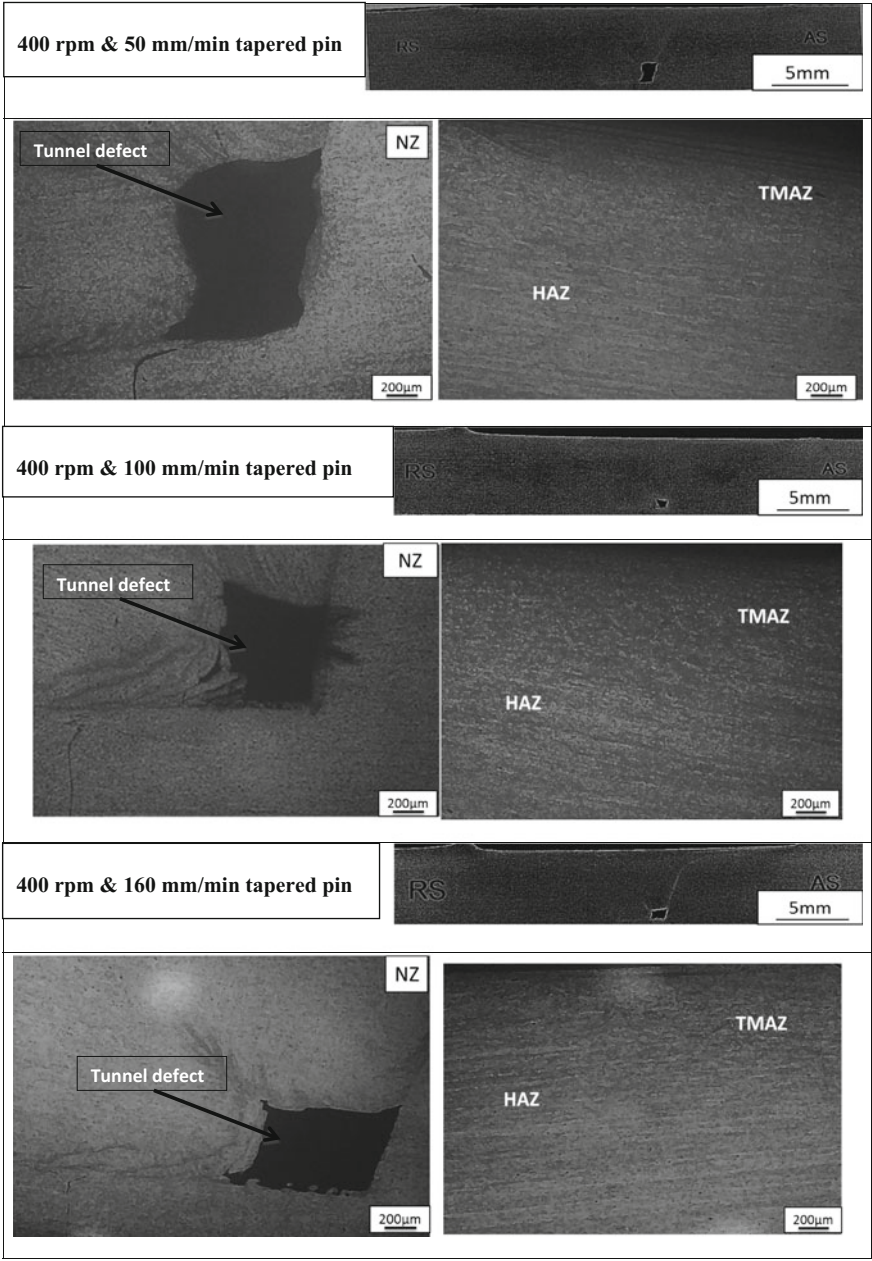


Fig. 11 (continued)

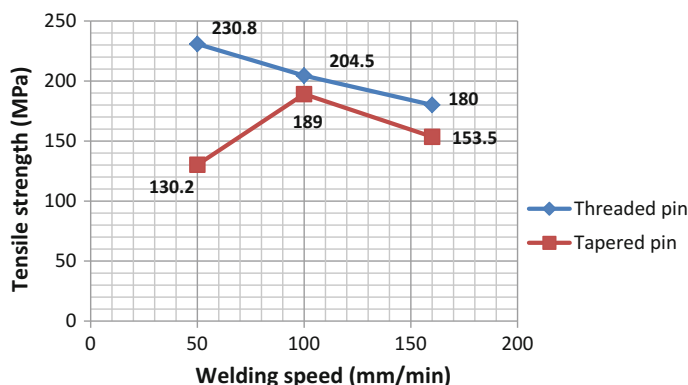


Fig. 12 The variation of TS with welding speed and pin profile at 400 rpm

profile tool at all welding speeds where, the largest tunnel defect size is at 50 mm/min welding speed and the smallest one is at 100 mm/min.

3.4 Mechanical Properties

The tensile strengths of the welded joints were obtained and plotted against welding speed for both types of tool pin profiles. As shown in Fig. 12 the best values of tensile strength are when using the threaded pin profile, especially at 50 mm/min welding speed; it is the best one. In comparison, using the tapered pin profile gives lower tensile strength values especially at 50 mm/min welding speed. It seems that the change in tool pin profile at 100 mm/min welding speed has a small effect on the tensile strength values.

Figure 13 shows the Vickers microhardness distribution along line perpendicular to the welding line at different FSW parameters. It is clear from graphs that for threaded cylindrical tool pin profile, the hardness values in nugget and thermo mechanically affected zones are greater than of base material at 50 and 100 mm/min welding speeds. The same is at 100 and 160 mm/min for tapered pin profile. This is due to finer grains in the welding zone. On the other hand, the hardness values are smaller than that of the base material 50 mm/min for tapered smooth tool pin profile and at some values for threaded pin profile at 160 mm/min welding speed. This action is due to coarsening of grains in the welding zone.

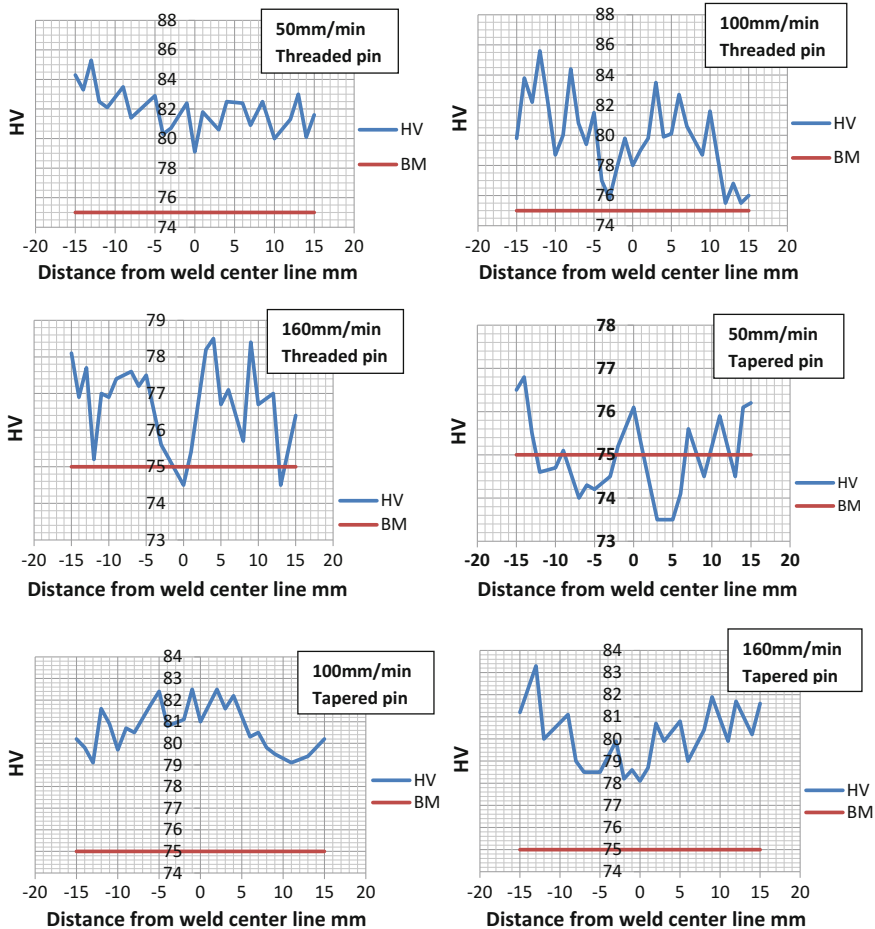


Fig. 13 Vickers microhardness distribution of the welded joints

4 Conclusions

Based on the present study, the following conclusions are obtained:

1. The peak temperature obtained from simulation is approximately near the measured one. Therefore, this heat transfer model can be used to predict the temperature distribution during the FSW process.
2. The peak temperature of the welded joints decreases by increasing the welding speed for the same tool pin profile and rotational speed.
3. Tool pin profile has a small effect on the peak temperature of the welded joints at the same welding speed.

4. The macrostructure and microstructure evolutions are affected by changing tool pin profile at the same welding speed.
5. Tensile strength values are affected by variations of the tool pin profile at the same welding speed.
6. Tensile strength values decrease by increasing welding speed for the joints welded by threaded tool pin profile.
7. The welded joints by threaded tool pin profile have an average hardness values in the welding zone greater than base material at all welding speed values.
8. The welded joints by tapered pin profile have an average value in the welding zone greater than base material at 100 or 160 mm/min welding speeds. While these values are lower than base material at 50 mm/min.

References

1. FSW-Technical-Handbook, ESAB, Welding Automation (2002) LAXÅ, Sweden
2. Thomas WM, Johnson KI, Wiesner CS (2003) Friction stir welding-recent developments in tool and process technologies. *Adv Eng Mater* 5:485–490
3. Mishra RS, Ma ZY (2005) Friction stir welding and processing. *Mater Sci Eng* 50:1–78
4. Rao MS, Prakash KJ, Kumar BVR (2013) A review of friction stir welding process and its variables. *Int J Sci Res (IJSR)* 2:375–379
5. Prasanna P, Penchalayya Ch, Rao DA (2013) Effect of tool pin profiles and heat treatment process in the friction stir welding of AA 6061. *Am J Eng Res (AJER)* 2:7–15
6. Threadgill PL, Leonard AJ, Shercliff HR, Withers PJ (2009) Friction stir welding of aluminum alloys. *Int Mater Rev* 54:49–93
7. Khodir SA, Shibayanagi T, Naka M (2006) Microstructure and mechanical properties of friction stir welded AA2024-T3 aluminum alloy. *Mater Trans* 47:185–193
8. Mao Y, Ke L, Liu F, Huang C, Chen Y, Liu Q (2016) Effect of welding parameters on microstructure and mechanical properties of friction stir welded joints of 2060 aluminum lithium alloy. *Int J Adv Manufact Technol* 81:1419–1431
9. Lim S, Kim S, Lee C, Kim S (2004) Tensile behavior of friction-stir-welded Al 6061-T651. *Metall Mater Trans* 35A:2829–2835
10. Habba MIA, Ahmed MMZ, Mohamed AYA, EL-Nikhaily A (2014) Effect of friction stir welding parameters on the mechanical properties of AA5083-H111. In: *Proceedings of the 10th international friction stir welding symposium*, Beijing, China
11. Chandrashekar A, Reddappa HN, Ajaykumar BS (2016) Influence of tool profile on mechanical properties of friction stir welded aluminum alloy 5083. *Int J Chem Mo Nucl Mater Metall Eng* 10:8–14
12. Schmidt H, Hattel J, Wert J (2004) An analytical model for the heat generation in friction stir welding. *Modell Simul Mater Sci Eng* 12:143–157
13. He X, Gu F, Andrew DB (2014) A review of numerical analysis of friction stir Welding. *Prog Mater Sci* 65:1–66

Improved Performance of Materials

Design and Experimental Approaches

Öchsner, A.; Altenbach, H. (Eds.)

2018, IX, 282 p. 179 illus., 116 illus. in color., Hardcover

ISBN: 978-3-319-59589-4